



Extracting Hale Cycle Related Components from Cosmic-Ray Data Using Principal Component Analysis

Jouni Takalo¹ 

Received: 31 January 2022 / Accepted: 3 August 2022
© The Author(s) 2022

Abstract

We decompose the monthly cosmic-ray data, using several neutron-monitor count rates, of Cycles 19–24 with principal component analysis (PCA). Using different cycle limits, we show that the first and second PC of cosmic-ray (CR) data explain 77–79% and 13–15% of the total variation of the Oulu CR Cycles 20–24 (C20–C24), 73–77% and 13–17% of the variation of Hermanus C20–C24, and 74–78% and 17–21% of the Climax C19–C22, respectively. The PC1 time series of the CR Cycles 19–24 has only one peak in its power spectrum at the period 10.95 years, which is the average solar-cycle period for SC19–SC24. The PC2 time series of the same cycles has a clear peak at period 21.90 (Hale cycle) and another peak at one third of that period with no peak at the solar-cycle period. We show that the PC2 of the CR is essential in explaining the differences in the intensities of the even and odd cycles of the CR. The odd cycles have a positive phase in the first half and a negative phase in the second half of their PC2. This leads to a slow decrease in intensity at the beginning of the cycle and a flat minimum for the odd cycles. On the contrary, for the even cycles the phases are reversed, and this leads to faster decrease and more rapid recovery of the CR intensity of the cycle. As a consequence, the even cycles have a more peak-like structure. These results are confirmed with skewness–kurtosis (S–K) analysis. Furthermore, S–K shows that other even and odd cycles, except Cycle 21, are on the regression line with a correlation coefficient 0.85. The Cycles 21 of all eight stations are compactly located in the S–K coordinate system and have smaller skewnesses and higher kurtoses than the odd Cycles 23.

Keywords Solar cycle · Cosmic rays · Corona · Solar wind, disturbances

1. Introduction

The neutron-monitor count rates have a known period of about 11 years, i.e. the average length of a solar cycle. However, it has been noticed that the cosmic-ray data experience also a 22-year or so-called Hale cycle, which is the magnetic polarity cycle of the Sun (Webber

✉ J. Takalo
jojuta@gmail.com

¹ Space Physics and Astronomy Research Unit, University of Oulu, POB 3000, FIN-90014, Oulu, Finland

and Lockwood, 1988; Mavromichalaki et al., 1997; Van Allen, 2000; Thomas, Owens, and Lockwood, 2014; Kane, 2014; Ross and Chaplin, 2019).

Webber and Lockwood (1988) found a sharply peaked CR-intensity maximum in 1987, similar to that observed 22 years earlier in 1965, in contrast to the flatter maximum observed between 1972 and 1977 and earlier, in 1952–1954. In addition, they found that the neutron-monitor (NM) count rate was about 1.5% higher at the times of maximum in 1965 and 1987 as compared with the 1972–1977 period.

Mavromichalaki et al. (1997) reported that in the CR odd cycles (C19 and C21) the decreasing of the intensity is slow and peaks shortly before the cycle minimum and has a saddle-like shape. In addition, odd cycles have a long recovery time and long temporal lag between CR and solar sunspot number (SSN). On the other hand, even CR cycles (C20 and C22) have a two-minima structure and overall peak-type structure. Furthermore, the even cycles have a rapid recovery phase and a short temporal lag to the SSN. They also studied the dependence of the CR as a function of SSN and found that the hysteresis curve between CR and SSN is more elliptic for the odd cycles than for the even cycles.

Van Allen (2000) confirms that there is a striking difference between such modulation loops, i.e. hysteresis curves between CR and SSN for solar-activity Cycles 19 and 21 and those for Cycles 20 and 22. The loops for Cycles 19 and 21 are broad ovals, whereas those for Cycles 20 and 22 are nearly flat. Furthermore, the cosmic-ray intensity decreases more rapidly as the SSN increases following solar-activity minima when the solar polar magnetic parameter $[A]$ is negative (magnetic moment and solar rotation axis are anti-parallel) than when A is positive (magnetic moment and rotation axis are parallel). He argues that these facts give some support to a significant role of gradient and curvature drifts in CR transport in the heliosphere.

Thomas, Owens, and Lockwood (2014) state that the onset of the peak cosmic-ray flux on Earth occurs earlier during $A > 0$ (odd) cycles than for $A < 0$ (even) cycles, and hence the peak is more dome-like for $A > 0$ and more sharply peaked for $A < 0$. They also demonstrate that these polarity-dependent heliospheric differences are evident during the space age, but are much less clear in earlier data. Using geomagnetic reconstructions, they show that for the period of 1905–1965, alternate polarities do not give as significant difference during the declining phase of the solar cycle. They suggest that the 22-year cycle in cosmic-ray flux is at least partly the result of direct modulation by the heliospheric magnetic field, and that this effect may be primarily limited to the grand solar maximum of the space age.

Owens et al. (2015) found that the approximately 22-year Hale cycle means that odd- and even-numbered Schwabe cycles, i.e. solar/sunspot cycles, are associated with different patterns in the galactic cosmic-ray intensity. They used recent ^{10}Be concentration measurements in their analysis.

Thomas et al. (2017) observe a difference in the phase and amplitude of the daily variation of neutron-monitor count rates with the Sun's magnetic polarity. The timing varies in a 22-year Hale cycle with maxima and minima latest in the solar minimum in $A < 0$ cycles and earliest in the solar minimum during $A > 0$ cycles.

Kane (2014) found that the hysteresis between cosmic-ray (CR) intensity (recorded at the Climax station) and sunspot number show broad loops in odd cycles (19, 21, and 23) and narrow loops in even cycles (20 and 22). However, in the even cycles, the loops are not narrow throughout the whole cycle; around the sunspot-maximum period, a broad loop is seen. The loops are narrow only in the rising and declining phases. Thus, the differences between odd and even cycles are not significant throughout the whole cycle. In the latest even cycle, i.e. Cycle 24, hysteresis plots show a preliminary broadening near the first sunspot maximum of 2012.

Ross and Chaplin (2019) show that plots of SSN versus GCR reveal a clear difference between the odd- and even-numbered cycles. Linear and elliptical models were fitted to the data, with the linear fit and elliptical model proving the more suitable model for even and odd solar-activity cycles, respectively, in agreement with the earlier studies. They study especially the lag and hysteresis of CR Cycle 24. They found that CR Cycle 24 has a slightly longer lag from SSN than previous even cycles. They suggest that the extended lag in Cycle 24 compared to previous even-numbered cycles is likely due to the deep, extended minimum between Cycles 23 and 24, and the low maximum activity of Cycle 24.

Mishra, Agarwal, and Tiwari (2008) found that the IMF velocity multiplied by the magnetic-field strength [vB] shows a weak negative correlation (-0.35) with cosmic rays for Solar Cycle 20, and a good anti-correlation for Solar Cycles 21–23 (-0.76, -0.69) with the cosmic-ray intensity.

Hempelmann and Weber (2012) used a Fourier analysis of the time series and suspected that the cosmic rays have a link with solar activity following their observations that showed significant peaks at 10.7, 22.4, and 14.9 years.

Broomhall (2017) modeled the hysteresis plots using both a simple linear model and an ellipse model, because of the difference in the shape of the hysteresis plots for odd and even cycles. The results of this study tend to support that Cycle 24 follows the same trend as preceding even cycles and is better represented by a straight line rather than an ellipse.

Oloketylui et al. (2020) found that CR intensity undergoes an 11-year solar cycle within the heliosphere, which is influenced mainly by solar activity. The cycle has its peak at the solar minimum. Their study also confirmed that the daily sunspot numbers and CRI are negatively correlated (correlation coefficient -0.72 for Cycle 23 and -0.73 for Cycle 24), i.e. anti-correlations observed are highly significant. Solar-wind speed was, however, found to be uncorrelated with SSN.

In this article, we use different methods from the earlier studies of CR cycles. We separate the solar-cycle related and Hale-cycle related components from the CR-flux data using principal component analysis (PCA). We show that the odd and even cycles differ in their second principal component (PC2). Furthermore, we show that also the skewness and kurtosis of the cycles separate even cycles, except Cycle 24, from the odd cycles. This article is organized as follows: Section 2 presents the data and methods used in this study. In Section 3, we present the results of PC and skewness–kurtosis analyses for CR data of Cycles 19–24 and discuss the results. We also make PC analyses of solar/solar-wind data and compare the results to those of CR data. We give our conclusion in Section 4.

2. Data and Methods

2.1. Cosmic-Ray Data

Although cosmic-ray intensity lags somewhat behind the solar sunspot numbers, we have used the dates in Table 1 for the cosmic-ray data cycles in the first PCA analysis. We used this choice first because the lags from solar cycles vary between different studies (Mavromichalaki et al., 1997; Gupta, Mishra, and Mishra, 2005; Rybanský, Kudela, and Minarovjech, 2009; Kane, 2014; Sierra-Porta, 2018; Iskra et al., 2019; Ross and Chaplin, 2019; Koldobskiy et al., 2022). We also varied the starting dates in order to see if this affected the results of the PC analysis. The other dates that we use in this article are the local maxima of different cosmic-ray cycles. These are shown in Table 2. We used in our analyses only cosmic-ray data that have at least four total cycles, excepting a few values missing due

Table 1 Sunspot-cycle lengths and dates of starting minima used in the first analysis.

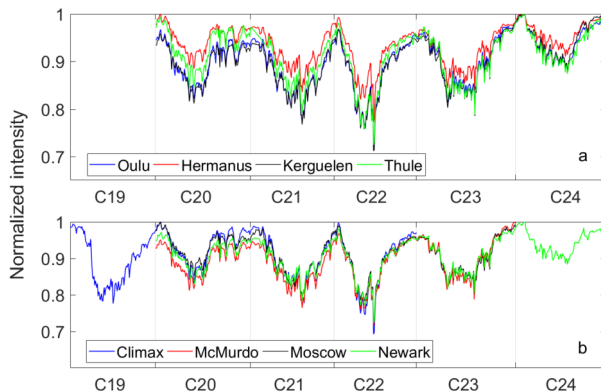
Sunspot-cycle number	Year and month of starting minimum	Cycle length [years]
19	1954 April	10.5
20	1964 October	11.7
21	1976 June	10.2
22	1986 September	10.1
23	1996 October	12.2
24	2008 December	11.0
25	2019 December	

Table 2 Cosmic-ray cycle lengths and dates of starting minima used for the second and third analyses.

Cycle number	Year and month of starting minimum	Cycle length [years]	Year and month of starting minimum	Cycle length [years]
19	1954 August	10.8	1955 April	10.8
20	1965 May	11.4	1965 December	11.4
21	1976 August	10.5	1977 April	10.0
22	1987 February	10.0	1987 April	10.8
23	1997 January	12.2	1998 January	11.8
24	2009 March	10.4	2009 December	10.3
25	2019 September		2020 March	

to gaps in the measurement. For this reason, we chose the Oulu CR flux as a primary data, because it consists of the five whole Cycles 20–24. We also study Hermanus and Climax CR as another primary data set, because the former station is located in the southern hemisphere and the latter is the only reliable station with continuous values for the whole Cycles 19–22. Note, however, that the early neutron monitors were more simple, called “IGY” type monitors, and only since 1964 the improved NM64 monitors have been used (Väisänen, Usoskin, and Mursula, 2021). For comparison for these data, we use data from Kerguelen (20–24), McMurdo (20–23), Moscow (20–23), Newark (20–24), and Thule (20–24). Figures 1a and b show the cosmic-ray intensities at the Oulu and Climax neutron-monitor stations for Cycles 20–24 and 19–22, respectively. We have added the other station to these figures (see captions of Figure 1). Because the cutoff rigidities and amount of NMs differ in different stations, i.e. the levels of the counts vary a lot (Usoskin et al., 2017; Väisänen, Usoskin, and Mursula, 2021), we normalize here the CR intensities such that the maximum of each station is unity. The normalization method does not affect the PCA because we do analyses for each station’s data separately. Note also from Figure 1 that the maxima of the CR intensities lag from the minima of the solar cycles shown as vertical lines. Another harmonization that we have to do is resampling (interpolation) of the cycles. This is because each cycle of the individual station must have the same length to be able to present the cycles as a correlation matrix, needed for the PCA. The cycles are, however, reverted to their original lengths and amplitudes after the PCA process.

Figure 1 The cosmic-ray data as normalized intensities for eight neutron-monitor (NM) stations.



2.2. Principal Component Analysis Method

Principal component analysis is a useful tool in many fields of science, including chemometrics (Bro and Smilde, 2014), data compression (Kumar, Rai, and Kumar, 2008), and information extraction (Hannachi, Jolliffe, and Stephenson, 2007). PCA finds combinations of variables that describe major trends in the data. PCA has earlier been applied, e.g., to studies of the geomagnetic field (Bhattacharyya and Okpala, 2015), geomagnetic activity (Holappa, Mursula, and Asikainen, 2014; Takalo, 2021b), the ionosphere (Lin, 2012), the solar background magnetic field (Zharkova et al., 2015), variability of the daily cosmic-ray count rates (Okpala and Okeke, 2014), and atmospheric correction to cosmic-ray detectors (Savić et al., 2019). As far as we know, this is the first time cosmic-ray cycles have been studied and compared using PCA.

To this end, we estimate that the average length of the cycle is 133 months (11.1 years) and use it as a representative cosmic-ray cycle. We first resample the monthly cosmic-ray counts such that all cycles have the same length of 133 time steps (months), i.e. about the average length of the Solar Cycles 20–24 (Takalo and Mursula, 2018, 2020; Takalo, 2021b). This effectively elongates or shortens the cycles to the same length. Before applying the PCA method to the resampled cycles, we standardize each individual cycle to have zero mean and unit standard deviation. This guarantees that all cycles will have the same weight in the study of their common shape. Then after applying the PCA method to these resampled and standardized cycles, we revert the cycle lengths and amplitudes to their original values.

Standardized data are then collected into the columns of the matrix \mathbf{X} , which can be decomposed as (Hannachi, Jolliffe, and Stephenson, 2007; Holappa et al., 2014; Takalo and Mursula, 2018)

$$\mathbf{X} = \mathbf{U} \mathbf{D} \mathbf{V}^T, \quad (1)$$

where \mathbf{U} and \mathbf{V} are orthogonal matrices, \mathbf{V}^T is a transpose of matrix \mathbf{V} , and \mathbf{D} is a diagonal matrix $\mathbf{D} = \text{diag}(\lambda_1, \lambda_2, \dots, \lambda_n)$ with λ_i the i th singular value of matrix \mathbf{X} . The principal components are obtained as the column vectors of

$$\mathbf{P} = \mathbf{U} \mathbf{D}. \quad (2)$$

The column vectors of the matrix \mathbf{V} are called empirical orthogonal functions (EOF) and they represent the weights of each principal component in the decomposition of the original

normalized data of each cycle X_i , which can be approximated as

$$X_i = \sum_{j=1}^N P_{ij} V_{ij}, \quad (3)$$

where j denotes the j th PC. The explained variance of each PC is proportional to square of the corresponding singular value λ_i . Hence the i th PC explains a percentage

$$\frac{\lambda_i^2}{\sum_{k=1}^n \lambda_k^2} 100\% \quad (4)$$

of the variance in the data.

2.3. Skewness and Kurtosis

The moments are a set of values that represent some important properties of the distributions. The most common are the first moment and the second moment, i.e. the expected value (mean value) and the variance. Two other important measures are the coefficients of skewness and kurtosis, i.e. third and fourth moments. The skewness measures the degree of asymmetry of the distribution, whereas kurtosis measures the degree of flatness of the distribution. The skewness can be defined as

$$\beta_1 = \frac{\sum_{i=1}^N (Y_i - \bar{Y})^3 / N}{s^3}, \quad (5)$$

where \bar{Y} is the mean, s is the standard deviation, i.e. the square root of the variance, and N is the number of data points. If skewness is positive/negative, the distribution is skewed to the right/left.

The kurtosis is defined as

$$\beta_2 = \frac{\sum_{i=1}^N (Y_i - \bar{Y})^4 / N}{s^4}. \quad (6)$$

Kurtosis is sometimes thought to tell us about the peakedness of the distribution, but it actually tells about the tails and flatness of the distribution. If kurtosis has a high/low value, it has heavy/light tails (Krishnamoorthy, 2006). The skewness–kurtosis pair of a normal distribution is (0, 3). That is why sometimes the coefficient “excess kurtosis” is used, i.e. the aforementioned kurtosis - 3.

3. Results and Discussion

3.1. PC Analyses

Using Oulu, Hermanus, and Climax cosmic-ray data, a PCA analysis was conducted by equalizing the cycles to 133 time steps (months) to get the two main principal components shown in Figure 2. The first and second PC explain 79.0% and 13.3% of the total variation of the Oulu C20–C24 data, 77.0% and 13.2% of the variation of Hermanus C20–C24, and 76.7% and 18.8% of the Climax C19–C22 data. Hence the two main PCs account together

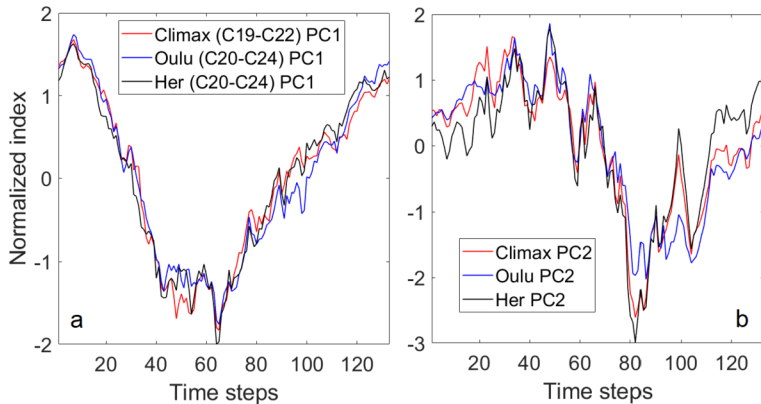
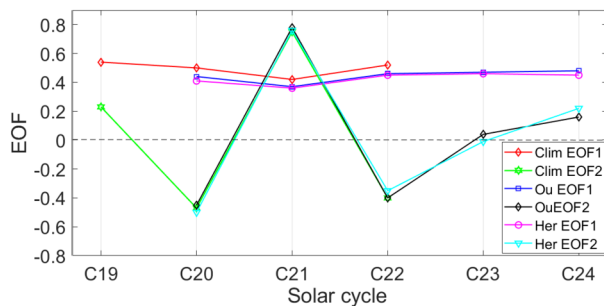


Figure 2 The PC1 in (a) and PC2 in (b) for the Oulu, Hermanus, and Climax cosmic-ray intensities of the first PC analysis.

Figure 3 The EOF1 and EOF2 of the Oulu, Hermanus, and Climax CR PC analyses.

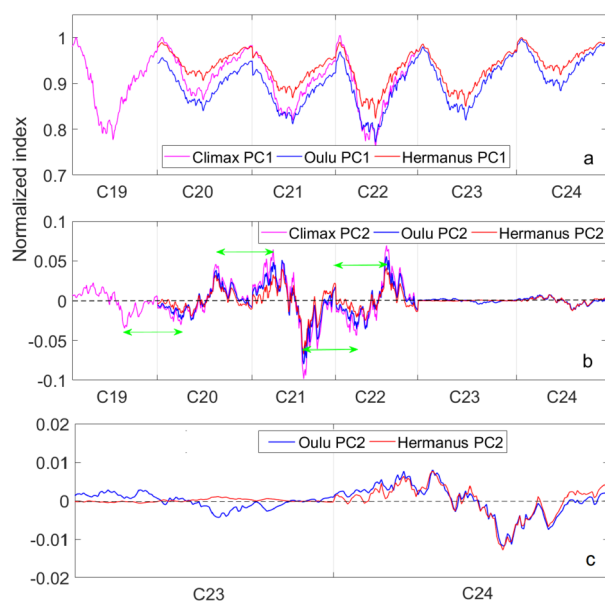


for 92.3%, 90.2%, and 95.5% of the total variation of CR data for Oulu, Hermanus, and Climax, respectively. Note, especially, that PC2 explains almost one-fifth of the Climax CR intensity.

Figure 3 shows the corresponding EOF of the Oulu, Hermanus, and Climax CR intensities. Note the almost sawtooth shape of the EOF2. The EOF2s of odd cycles are positive and EOFs of even cycles are negative, except for EOF2 of Cycle 24 of Oulu and Hermanus, which have opposite sign to those for earlier even cycles. Note also that EOF2 for the Hermanus Cycle 23 is slightly negative, in contrast to other odd cycles. Looking at the shape of PC2 in Figure 2, we note that a positive EOF2 means a positive phase in the first half of the cycle and a negative phase in the second half of the cycle. For a negative EOF2, the phases are opposite. Note the similarity of the EOF1 and EOF2 in the cycles, which are common for all stations. EOF1s for Climax are a little higher because the PCA is calculated from only four cycles, while Oulu and Hermanus PCA are calculated from five cycles. It is essential, that Cycle 21 has the lowest weight to all PC1s, but the highest weight to the all PC2. (Later, we call PC2 phase positive if it starts with a positive phase (as in Figure 2b), and negative if it starts with a negative phase.)

Reverting the PC1, PC2 cycles of Oulu, Hermanus, and Climax CR back to their original length and concatenating them, we get first and second principal component time series for the CR cycles, shown in Figure 4a and Figure 4b, respectively (we still use the same normalization as in the Figure 1). It is evident that PC1 is dominated by the sunspot cycle

Figure 4 (a) PC1 and (b) PC2 time series of the PCA of CR intensities of Oulu, Hermanus, and Climax for Cycles 19–24. (c) magnification of C23 and C24 for Oulu and Hermanus.



related period. Interestingly, the largest size of PC1 is almost equal for Cycles 19 and 22, and the smallest for Cycles 20 and 24.

In contrast to PC1, PC2 shows a clear Hale cycle period (see Figure 4b). Note that the consecutive even–odd cycle pairs show similar structure for two Hale cycles. The Hale cycle is traditionally described as an even–odd cycle pair (Gnevyshev and Ohl, 1948; Wilson, 1988; Makarov, 1994; Cliver, Boriakoff, and Bounar, 1996; Takalo, 2021b). However, we start here with odd Cycle 19, because this is the first cycle with cosmic-ray measurements. Note that cycle pairs 19–20 and 21–22 have opposite phases, i.e. the first cycle is positive and the second cycle is negative. Note also a very strong peak-to-peak variation of the Cycle 21 PC2, and also quite strong variation of the Cycle 22 PC2. After that, the situation changes such that Cycle 23 is still positive for Oulu, as expected for the odd cycle, but slightly negative for Hermanus. Cycle 24 is again positive for both Oulu and Hermanus CR PC2 time series. There really is a change from the patterns of earlier odd–even cycle pairs.

In Figures 5a and b we show the PC1 and PC2 timeseries of the other station we have studied. They seem very similar to the PCs of Oulu CR for Cycles 20–24. Note, especially, that the positive phase (seen clearly in magnification) for Cycle 23 is slightly greater for Moscow and Thule than for the other CR stations. This is also the case for Thule in Cycle 24, so it seems there is no bias just in Cycle 23. The cosmic-ray data of Moscow was somewhat biased for the Cycle 24, which would have distorted the whole PCA for Moscow. That is why we omitted the Cycle 24 data for Moscow.

Figures 6a, b, and c show the original CR intensities and PC1+PC2 proxy time series for Oulu and Climax and Hermanus stations, respectively. The main features are reproduced by these two main PCs quite well, especially for Climax data. The clearest differences are in Cycle 23 for the Oulu and Hermanus data. The late peaks and fast recovery after them do not arise from the PC1 and PC2. These features, which are unique for one cycle alone, are produced by the higher-order PCs. Cycle 23 has a large value for EOF3 and when we add the PC3, i.e. plot PC1+PC2+PC3, the aforementioned features are corrected quite well (green curve in Figure 6a). Note that Cycle 22 does not change at all when PC3 is added,

Figure 5 (a) PC1 and (b) PC2 time series of the PCA of CR intensities of Newark, Kerguelen, Thule, McMurdo, and Moscow. (c) magnification of Cycles 23 and 24.

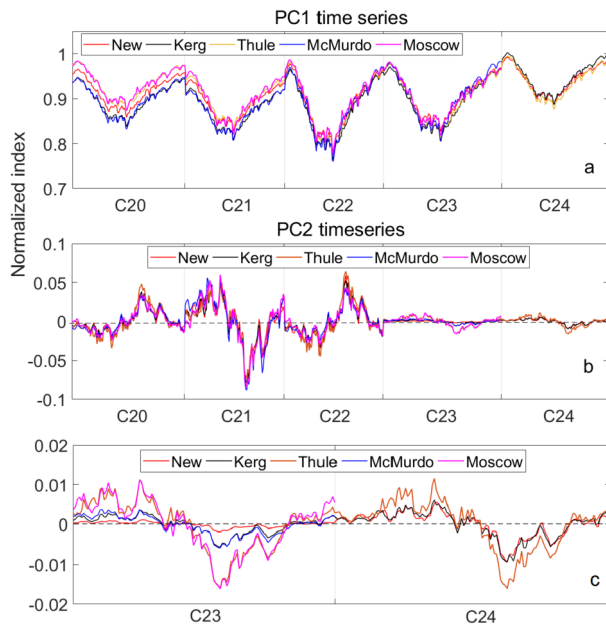
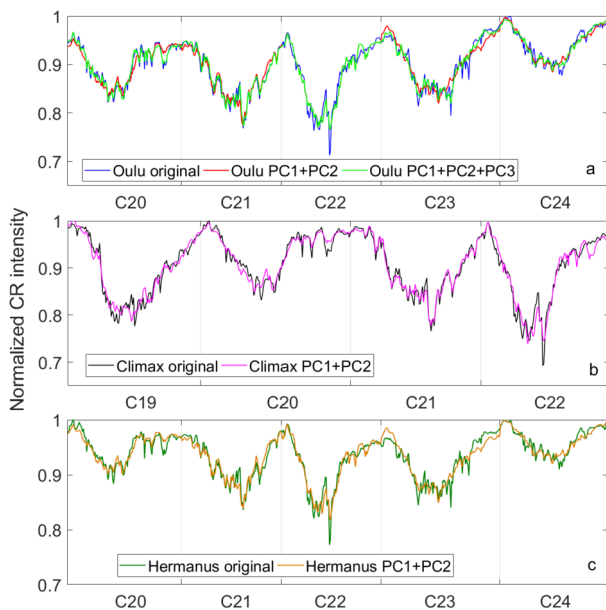


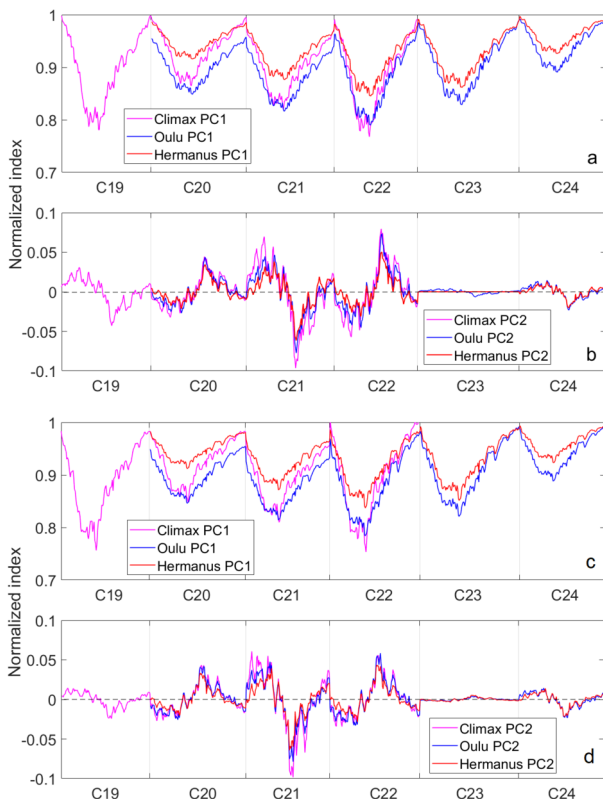
Figure 6 (a) Original monthly CR time series for Oulu C20–C24 (blue), their PC1+PC2 proxy (red) and PC1+PC2+PC3 proxy (green) time series. (b) Original monthly CR time series for Climax C19–C22 (black) and their PC1+PC2 proxy time series (magenta). (c) Original monthly CR time series for Hermanus C20–C24 (green) and its PC1+PC2 proxy time series (brown).



and the green PC1+PC2+PC3 proxy curve is on top the red line for C22. This is because its EOF3 for C22 is practically zero. The case is similar for the Hermanus station.

In order to see if the choice of the starting minima (and the length of the cycle) of the cosmic-ray cycles affects the PC analysis, we used the dates of the starting minima shown in Table 2. It is also a well-known fact that cosmic-ray flux lags the solar-activity cycle from a few months to over a year depending on the station and cycle (Mavromichalaki et al., 1997;

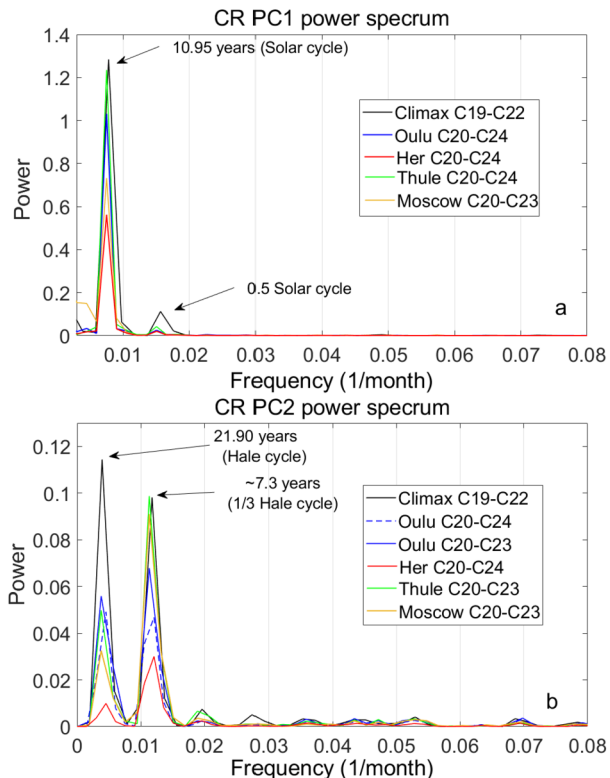
Figure 7 (a) PC1 and (b) PC2 time series of CR intensities for Oulu, Hermanus, and Climax for Cycles 19–24 of the second PC analysis (c) PC1 and (d) PC2 time series of CR intensities for Cycles 19–24 of the third PC analysis.



Gupta, Mishra, and Mishra, 2005; Rybanský, Kudela, and Minarovjech, 2009; Kane, 2014; Sierra-Porta, 2018; Iskra et al., 2019; Ross and Chaplin, 2019; Koldobskiy et al., 2022). In the second analysis, the PC1 and PC2 explain 78.1% and 14.4% of the total variation in the Oulu C20–C24 data, 74.9% and 15.3% of the variation of Hermanus C20–C24, and 74.5% and 20.4% of the Climax C19–C22 data. Hence the two main PCs account together for almost the same part of the total variation in the CR data as in the first analysis, i.e. 92.5%, 90.2% and 94.9% for Oulu, Hermanus, and Climax, respectively. Figures 7a and b show the corresponding time series of PC1 and PC2, respectively. In the third analysis, we used still larger time lags and these starting dates are also available in Table 2. In the third analysis, PC1 and PC2 explain 77.3% and 15.2% (together 92.5%) of the total variation of the Oulu C20–C24 data, 73.3% and 16.6% (together 89.9%) of the variation of Hermanus C20–C24 and 78.3% and 17.5% (together 95.8%) of the Climax C19–C22 data. Figures 7c and d show the corresponding time series of PC1 and PC2, respectively. Note the similarity of this figure with Figures 4a and b, and 7a and b, although the cycle starting dates now differ from 4 to 14 months from the sunspot-cycle starting dates. The most striking difference in the last PC2 compared to earlier PC2s is that even Oulu now has a slightly negative phase for the odd Cycle 23. This result confirms the statement that Cycle 23 is more similar to earlier even cycles than to the odd cycles.

Figures 8a and b show the power spectra of PC1 and PC2 time series of Figures 4a and b, respectively. It is clear that PCA effectively decomposes the solar-cycle and Hale-cycle related periods from the CR data. According to these spectra the solar-cycle period is 10.95 years (on the average) and the Hale cycle about 21.9 years. In the Figure 8b, there is another

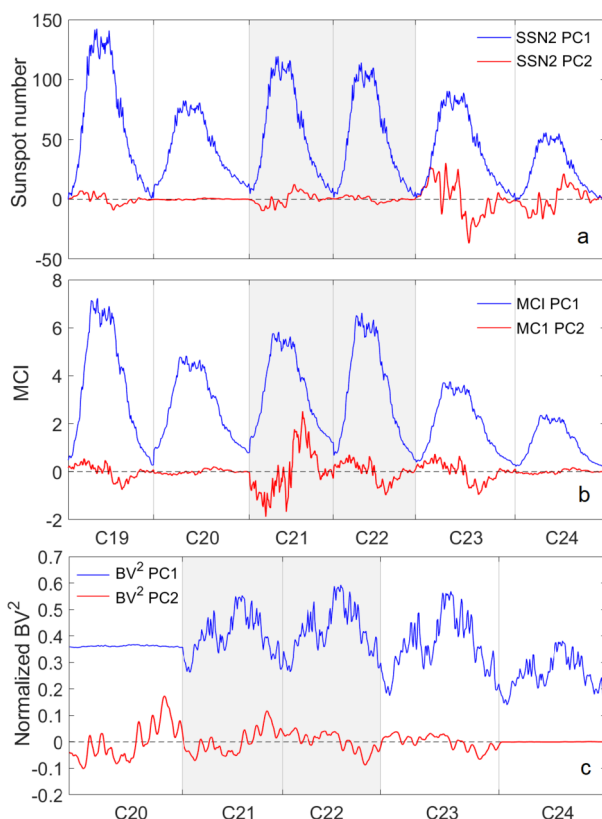
Figure 8 The power spectra of the (a) PC1 and (b) PC2 time series of Figure 4.



smaller peak at a period of one-third of the Hale cycle. We believe that this peak is related to the phase change between the succeeding cycles, so that the maxima (or minima) of the PC2 are separated by about two-thirds of the solar-cycle (marked with two-headed arrows in Figure 4b) from each other. In the Figure 8b there are two spectra of Oulu PC2. The dashed-blue spectral peaks are for the whole period C20–C24, and the solid-blue spectral peaks are for the case where the last Cycle 24, with “wrong phase” omitted from the spectral analysis. We have added power spectra of Thule and Moscow for C20–C23 to the Figure 8 to confirm that the peaks are the same (it is not necessary to show all the power spectra, because Figure 5 shows that the PC1s and PC2 are very similar at all stations). The one-third of Hale cycle peak is even stronger than the whole-cycle peak for Oulu, Hermanus, Thule, and Moscow. We suppose that this is due to strong peaks for PC2 of the Cycles 20–22 for all these stations. However, this peak is somewhat artificial, because it comes from the concatenation of the separate PC2s of the different cycles. The important thing is that we have removed solar-cycle related period from the CR data. Note that for Climax the whole Hale-cycle peak is higher than the one-third Hale-cycle peak, because Climax CR data consist of only the distinct Hale-cycle pairs 19–20 and 21–22.

We can now compare our results with the earlier studies. The positive PC2, i.e. positive phase in the first half of the cycle, means that the decrease in the CR intensity is slower than if it were negative. In Figures 4 and 5 we see that this is the case for odd cycles. This result is similar to those of, e.g., Mavromichalaki et al. (1997) and Van Allen (2000). For the even Cycles 20 and 22, the first half of PC2 has a negative phase and the second half has a positive phase. This makes the decline of the CR cycle faster and the recovery more rapid leading

Figure 9 The PC1s and PC2s of (a) sunspot numbers and (b) monthly corona indices for Solar Cycles 19–24. (c) The PC1 and PC2 for solar wind/IMF function Bv^2 of Solar Cycles 20–24.



to more peak-like structure of the even cycles. That was the result of the earlier studies too: see Webber and Lockwood (1988), Mavromichalaki et al. (1997), Van Allen (2000), and Thomas, Owens, and Lockwood (2014). We have shown here the essential reason for these behaviors in CR, i.e. they are caused by the Hale-cycle related component of the CR data.

We have also conducted a PC analysis for sunspot number 2.0 monthly data (SSN), solar monthly corona index (MCI), and a function proportional to the IMF magnetic-field intensity multiplied by the square of the solar-wind velocity [Bv^2]. The last one has been shown to play the central role in the process of energy transfer (Ahluwalia, 2000; Verbanac et al., 2011; Takalo, 2021a). Figures 9a, b, and c show the PC1 and PC2 timeseries for SSN, MCI, and Bv^2 , respectively. Note that OMNI data, which are used to calculate Bv^2 exist only since 1964, i.e. for Solar Cycles 20–24. (The PC2s have been slightly smoothed to better see the phases of the cycles.) Note that PC2s are in the same phase for all solar/IMF parameters. We would assume that the solar parameters anti-correlate with cosmic-ray data. Indeed, PC2 of the Cycles 21 and 22 (marked in gray) are exactly in opposite phase with the PC2 of the cosmic-ray data. Note that PC2 is by far the strongest for just these cycles in CR data. The solar-wind speed and consequently Bv^2 seem to be always stronger in the latter half of the cycle, i.e. during the descending phase of the solar cycle (see Figure 9c) (Takalo, 2021a). We would then suppose that cosmic-ray intensity has negative phase as preferred state in the second half of the cycle. This is actually the case for Cycles 23 and 24 (instead slightly for Hermanus C23 and in one case for Oulu). Although we do not have solar-wind data for Cycle 19, the situation could be the same for this cycle also. Cycle 20

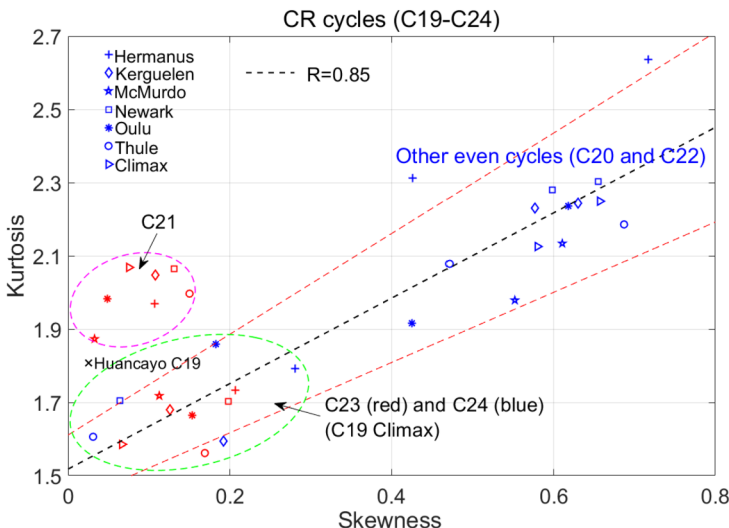


Figure 10 The skewness–kurtosis coordinate map shows these parameters for the Cycles 19–24 of all stations analysed in this study.

is the only one which does not fit in to the aforementioned pattern. Note, however, that the Bv^2 PC1 is totally different for Cycle 20 than the other cycles. The PC1 for Cycle 20 is almost constant and the stronger second half rather exists in the PC2 for this cycle. Agarwal and Mishra (2008) already found that the interplanetary magnetic-field strength [B] shows only a weak negative correlation (-0.35) with cosmic rays for Solar Cycle 20, whereas it shows a high anti-correlation for the Solar Cycles 21–23 (-0.76, -0.69). They suspect that a significant contribution to modulation from the termination shock during Solar Cycle 20 could dilute the correlation of cosmic rays with the interplanetary magnetic field B at one astronomical unit for that cycle. The perturbations of the heliosphere are weaker and less widely spread during Solar Cycle 20 than during other solar cycles. This might lead to a situation where the heliospheric perturbations are relatively small for cosmic-ray particles, allowing these particles to reach the Earth as if it were a minimum solar-activity period. Note from Figure 4a that the decrease of the cosmic-ray intensity is smaller for Cycle 20 than for Cycle 23, especially for Hermanus, although the sunspot numbers are almost the same for these cycles and the solar corona is even stronger for Cycle 20 than for Cycle 23 (see Figure 9).

3.2. Skewness and Kurtosis of the Cycles

We calculated skewnesses and kurtoses of CR Cycles 19–22 for Climax and Cycles 20–24 for Hermanus, Kerguelen, McMurdo, Newark, Oulu, and Thule. Figure 10 shows the result in the skewness–kurtosis (S–K) coordinate system. There are several interesting features. The cycles other than C21 are near the regression line (shown as a black-dashed line), so that Cycles 23 and 24 are in the lower-left corner, meaning small skewness and low kurtosis. Interestingly, Cycle 19 for Climax is among Cycles 23 and 24 in the lower-left ellipse. The even Cycles 20 and 22 are in the upper-right corner with larger skewness and higher kurtosis. The correlation coefficient of the regression line is 0.85 and 95% confidence limits are shown as red-dashed lines. Note that only even Cycles 20 and 22 for Hermanus are somewhat

outside the 95% limits. Cycles 21 are omitted from this regression, and their results are located compactly inside a small ellipse with small skewness and moderate kurtosis. We should remember that the Cycle 21 differed from others in PCA such that its weight for PC1 is smallest and PC2 highest of all cycles. Another classification could be that all odd cycles plus Cycle 24 have small skewness and even Cycles 20 and 22 have moderate to large skewness. The skewness–kurtosis map also shows that Cycle 21 differs from others such that they are compactly located in a small area in this coordinate system. Also the skewness–kurtosis values for another odd Cycle 23 form a quite compact group, but with somewhat lower kurtosis and slightly larger skewness. The interesting thing is that Cycle 19 has almost the smallest value for skewness and kurtosis of all cycles. It is a pity that we do not have any other results for the whole of Cycle 19, and even these data were measured with the old IGY-type monitor. There exists another whole Cycle 19 measured at Huancayo, and we have marked it as an “x” to the skewness–kurtosis coordinate map. Its skewness is almost zero and it is located near the Cycles 21 in the S–K map. The other cycles for Huancayo C20 and C21 are, however, so flat, i.e. have such heavy tails, that their kurtosis is outside the S–K map of Figure 10. The reason is probably the very high rigidity cutoff for that station, 13.4 GeV, and thus its insensitivity to low-energy cosmic rays (Usoskin et al., 2001, 2017). Another reason to omit Huancayo in PCA is that there exist only three whole cycles for this station.

4. Conclusion

We have studied CR fluxes of several stations using PC analyses. We present the PCA of Climax CR for Cycles 19–23 and Hermanus and Oulu CR for Cycles 20–24 in more detail. We found that the first and second PC explain 76.7% and 18.8%, 77.0% and 13.2%, and 79.0% and 13.3% of the total variation of the Climax, Hermanus, and Oulu CR flux data, respectively. This means that only the two main PCs account for 95.5%, 90.2% and 92.3% of the total variation of Climax, Hermanus, and Oulu CR intensity, respectively. The results for the time-lagged analyses (second and third PCA) give compatible results with similar significance of their PC1 and PC2. We have also shown that PC1 is related to the solar cycle and PC2 is related to the Hale cycle, i.e. in the latter there is no solar-cycle-related peak in the power spectrum. According to PCA, the normalized principal components are perpendicular to each other. Note that almost one-fifth of the Climax data are related to the 22-year magnetic-polarity cycle (for the second analysis over 20%). This is likely due to the presence of grand-solar-maximum cycles in Climax data. For Hermanus and Oulu the percentage is lower, because there are the weak Cycles 23 and 24 included in the analysis. The polarity of the heliospheric magnetic field seems to have a very important role in the intensity of CR fluxes, at least during the grand solar maximum. We have also shown that especially the PC2s of three solar related parameters SSN, SCI, and Bv^2 are for Cycles 21 and 22, i.e. for a whole odd–even Hale cycle, in opposite phase with the cosmic-ray PC2.

Our study shows that Cycle 23 is different from earlier odd cycles in that it has very weak positive phase in its PC2, and even slightly negative for the southern-hemisphere station Hermanus in the second and third analyses, and for northern-hemisphere Oulu in the third analysis. Interestingly, Cycle 24 differs from the earlier even Cycles 20 and 22 such that it has a positive phase in its PC2 in all analyses, and this is even stronger than for odd Cycle 23. Furthermore, Cycles 23 and 24 are very near each other in the skewness–kurtosis map with small skewness and low kurtosis values. On the other hand, all other even cycles have larger skewnesses and higher kurtoses. CR Cycles 21 differ from Cycles 23 such that their

kurtoses are higher and they do not match the regression line, which combines the other odd and even cycles with a correlation coefficient 0.85. Cycle 19 is somewhat problematic with inadequate cosmic-ray data.

The aforementioned analysis leads us to conclude that the clear Hale cycle in cosmic-ray data, so that succeeding cycles are in different phases, may occur only for solar cycles of the grand-maximum during the second half of the 20th century (Thomas, Owens, and Lockwood, 2014). Another explanation could be that there is a phase shift, which started during Cycle 23 (McDonald, Webber, and Reames, 2010) and went on during Cycle 24, and the phases of even and odd cycles are changing places. We, however, rather suppose that while the solar-wind function Bv^2 was usually stronger in the descending phase of the solar cycle (see Figure 9c PC1), due to high-speed streams (Gosling, Asbridge, and Bame, 1977; Simon and Legrand, 1989; Cliver, Boriakoff, and Bounar, 1996; Echer et al., 2004), it is the cause for positive phase in the first half and negative phase in the second half of the PC2 for the weaker solar cycles such as C23 and C24.

Acknowledgments I acknowledge the NMDB database (www.nmdb.eu), founded under the European Union's FP7 programme (contract no. 213007), and the teams of the Climax, Hermanus, Kerguelen, McMurdo, Moscow, Newark, Oulu and Thule neutron monitors for providing data. The neutron-monitor data from McMurdo, Newark/Swarthmore, and Thule were provided by the University of Delaware Department of Physics and Astronomy and the Bartol Research Institute. Kerguelen neutron monitor data were kindly provided by the Observatoire de Paris and the French Polar Institute (IPEV), France. The Oulu NM is operated by Sodankyla Geophysical Observatory of the University of Oulu. The Moscow Neutron Monitor is operated by the Pushkov Institute of Terrestrial Magnetism, Ionosphere and Radio Wave propagation (IZMIRAN) of the Russian Academy of Science. The Hermanus NM is attended by the South African National Space Agency. The SSN 2.0 data are fetched from www.bis.sidc.be/silso/datafiles, the monthly solar corona data from www.ngdc.noaa.gov/stp/solar/corona.html, and the OMNI2 data from spdf.gsfc.nasa.gov/pub/data/omni/low_res_omni/. I am also grateful to I. Usoskin for useful communications.

Funding Note Open Access funding provided by University of Oulu including Oulu University Hospital.

Data Availability All the data used can be downloaded from the aforementioned web-pages.

Declarations

Disclosure of Potential Conflicts of Interest The author declares that there are no conflicts of interest.

Open Access This article is licensed under a Creative Commons Attribution 4.0 International License, which permits use, sharing, adaptation, distribution and reproduction in any medium or format, as long as you give appropriate credit to the original author(s) and the source, provide a link to the Creative Commons licence, and indicate if changes were made. The images or other third party material in this article are included in the article's Creative Commons licence, unless indicated otherwise in a credit line to the material. If material is not included in the article's Creative Commons licence and your intended use is not permitted by statutory regulation or exceeds the permitted use, you will need to obtain permission directly from the copyright holder. To view a copy of this licence, visit <http://creativecommons.org/licenses/by/4.0/>.

References

Agarwal, R., Mishra, R.K.: 2008, Solar cycle phenomena in cosmic ray intensity up to the recent solar cycle. *Phys. Lett. B* **664**, 31. [DOI](#).

Ahluwalia, H.S.: 2000, Galactic cosmic ray diurnal modulation, interplanetary magnetic field intensity and the planetary index *Ap. Geophys. Res. Lett.* **27**, 617. [DOI](#).

Bhattacharyya, A., Okpala, K.C.: 2015, Principal components of quiet time temporal variability of equatorial and low-latitude geomagnetic fields. *J. Geophys. Res.* **120**, 8799. [DOI](#).

Bro, R., Smilde, A.K.: 2014, Principal component analysis. *Anal. Methods* **6**, 2812.

Broomhall, A.M.: 2017, A helioseismic perspective on the depth of the minimum between solar cycles 23 and 24. *Solar Phys.* **292**, 2812. [DOI](#).

Cliver, E.W., Boriakoff, V., Bounar, K.H.: 1996, The 22-year cycle of geomagnetic and solar wind activity. *J. Geophys. Res.* **101**, 27091. [DOI](#). [ADS](#).

Echer, E., Gonzalez, W.D., Gonzalez, A.L.C., Prestes, A., Vieira, L.E.A., Dal Lago, A., Guarneri, F.L., Schuch, N.J.: 2004, Long-term correlation between solar and geomagnetic activity. *J. Atmos. Solar-Terr. Phys.* **66**, 1019. [DOI](#). [ADS](#).

Gnevyshev, M.N., Ohl, A.I.: 1948, On the 22-year cycle of solar activity. *Astron. Zh.* **25**, 18.

Gosling, J.T., Asbridge, J.R., Bame, S.J.: 1977, An unusual aspect of solar wind speed variations during solar cycle 20. *J. Geophys. Res.* **82**, 3311. [DOI](#). [ADS](#).

Gupta, M., Mishra, V.K., Mishra, A.P.: 2005, Correlative study of solar activity and cosmic ray intensity for solar cycles 20 to 23. In: Sripathi, A., Gupta, S., Jagadeesan, P., Jain, A., Karthikeyan, S., Morris, S., Tonwar, S. (eds.) *Proc. 29th Internat. Cosmic Ray Conf.* **2**, Tata Institute of Fundamental Research, Mumbai, 147.

Hannachi, A., Jolliffe, I.T., Stephenson, D.B.: 2007, Empirical orthogonal functions and related techniques in atmospheric science: A review. *Int. J. Climatol.* **27**, 1119. [DOI](#).

Hempelmann, A., Weber, W.: 2012, Correlation between the sunspot number, the total solar irradiance, and the terrestrial insolation. *Solar Phys.* **277**, 417. [DOI](#).

Holappa, L., Mursula, K., Asikainen, T.: 2014, A new method to estimate annual solar wind parameters and contributions of different solar wind structures to geomagnetic activity. *J. Geophys. Res.* **119**, 9407. [DOI](#). [ADS](#).

Holappa, L., Mursula, K., Asikainen, T., Richardson, I.G.: 2014, Annual fractions of high-speed streams from principal component analysis of local geomagnetic activity. *J. Geophys. Res.* **119**, 4544. [DOI](#). [ADS](#).

Iskra, K., Siluszyk, M., Alania, M., Wozniak, W.: 2019, Experimental investigation of the delay time in galactic cosmic ray flux in different epochs of solar magnetic cycles: 1959–2014. *Solar Phys.* **294**, 115. [DOI](#). [ADS](#).

Kane, R.P.: 2014, Lags and hysteresis loops of cosmic ray intensity versus sunspot numbers: Quantitative estimates for cycles 19–23 and a preliminary indication for cycle 24. *Solar Phys.* **289**, 2727. [DOI](#).

Koldobskiy, S.A., Kähkönen, R., Hofer, B., Krivova, N.A., Kovaltsov, G.A., Usoskin, I.G.: 2022, Time lag between cosmic-ray and solar variability: Sunspot numbers and open solar magnetic flux. *Solar Phys.* **297**, 18. [DOI](#).

Krishnamoorthy, K.: 2006, *Handbook of Statistical Distributions with Applications*, Chapman & Hall, Boca Raton.

Kumar, D., Rai, C.S., Kumar, S.: 2008, Principal component analysis for data compression and face recognition. *INFOCOMP J. Comput. Sci.* **7**, 48.

Lin, J.-W.: 2012, Ionospheric total electron content seismo-perturbation after Japan's March 11, 2011, M=9.0 Tohoku earthquake under a geomagnetic storm; a nonlinear principal component analysis. *Astrophys. Space Sci.* **341**, 251. [DOI](#).

Makarov, V.I.: 1994, Global magnetic activity in 22-year solar cycles. *Solar Phys.* **150**, 359. [DOI](#). [ADS](#).

Mavromichalaki, H., Belehaki, A., Rafios, X., Tsagouri, I.: 1997, Hale-cycle effects in cosmic-ray intensity during the last four cycles. *Astrophys. Space Sci.* **246**, 7.

McDonald, F.B., Webber, W., Reames, D.V.: 2010, Unusual time histories of galactic and anomalous cosmic rays at 1 AU over the deep solar minimum of cycle 23/24. *Geophys. Res. Lett.* **37**, L18101. [DOI](#).

Mishra, R.K., Agarwal, R., Tiwari, S.: 2008, Solar cycle variation of cosmic ray intensity along with interplanetary and solar wind plasma parameters. *Latv. J. Phys. Tech. Sci.* [DOI](#).

Okpalak, K., Okeke, F.: 2014, Variability of the daily cosmic ray count rates in the northern hemisphere. In: Willis, P. (ed.) *40th COSPAR Sci. Assemb.* **40**, D1.3.

Oloketylui, J., Liu, Y., Amanambu, A.C., Zhao, M.: 2020, Responses and periodic variations of cosmic ray intensity and solar wind speed to sunspot numbers. *Adv. Astron.* **2020**, 3527570. [DOI](#). [ADS](#).

Owens, M.J., McCracken, K.G., Lockwood, M., Barnard, L.: 2015, The heliospheric Hale cycle over the last 300 years and its implications for a “lost” late 18th century solar cycle. *J. Space Weather Space Clim.* **5**, A30. [DOI](#). [ADS](#).

Ross, E., Chaplin, W.J.: 2019, The behaviour of galactic cosmic-ray intensity during solar activity cycle 24. *Solar Phys.* **294**, 8. [DOI](#).

Rybanský, M., Kudela, K., Minarovjech, M.: 2009, Solar corona and cosmic rays 1953 - 2008. In: Szabelski, J., Giller, M. (eds.) *Proc. 31th Internat. Cosmic Ray Conf.*, University of Łódź, Łódź.

Savić, M., Dragić, A., Maletić, D., Veselinović, N., Banjanac, R., Joković, D., Uđovičić, V.: 2019, A novel method for atmospheric correction of cosmic-ray data based on principal component analysis. *Astropart. Phys.* **109**, 1.

Sierra-Porta, D.: 2018, Cross correlation and time-lag between cosmic ray intensity and solar activity during solar cycles 21, 22 and 23. *Astrophys. Space Sci.* **363**, 137. [DOI](#).

Simon, P.A., Legrand, J.P.: 1989, Solar cycle and geomagnetic activity: A review for geophysicists. Part 2. The solar sources of geomagnetic activity and their links with sunspot cycle activity. *Ann. Geophys.* **7**, 579. [ADS](#).

Takalo, J.: 2021a, Comparison of geomagnetic indices during even and odd solar cycles SC17-SC24: Signatures of Gnevyshev gap in geomagnetic activity. *Solar Phys.* **296**, 19. [DOI](#).

Takalo, J.: 2021b, Separating the aa-index into solar and Hale cycle related components using principal component analysis. *Solar Phys.* **296**, 80. [DOI](#).

Takalo, J., Mursula, K.: 2018, Principal component analysis of sunspot cycle shape. *Astron. Astrophys.* **620**, A100. [DOI](#).

Takalo, J., Mursula, K.: 2020, Comparison of the shape and temporal evolution of even and odd solar cycles. *Astron. Astrophys.* **636**, A11. [DOI](#).

Thomas, S.R., Owens, M.J., Lockwood, M.: 2014, The 22-year Hale cycle in cosmic ray flux – Evidence for direct heliospheric modulation. *Solar Phys.* **289**, 407. [DOI](#).

Thomas, S., Owens, M., Lockwood, M., Owen, C.: 2017, Decadal trends in the diurnal variation of galactic cosmic rays observed using neutron monitor data. *Ann. Geophys.* **35**, 825. [DOI](#). [ADS](#).

Usoskin, I.G., Bobik, P., Gladysheva, O.G., Kananen, H., Kovaltsov, G.A., Kudela, K.: 2001, Sensitivity of a neutron monitor to galactic cosmic rays. *Adv. Space Res.* **27**, 565. [DOI](#). [ADS](#).

Usoskin, I.G., Gil, A., Kovaltsov, G.A., Mishev, A.L., Mikhailov, V.V.: 2017, Heliospheric modulation of cosmic rays during the neutron monitor era: Calibration using PAMELA data for 2006–2010. *J. Geophys. Res.* **122**, 3875. [DOI](#).

Väistönen, P., Usoskin, I., Mursula, K.: 2021, Seven decades of neutron monitors (1951–2019): Overview and evaluation of data sources. *J. Geophys. Res.* **126**, e2020JA028941. [DOI](#).

Van Allen, J.A.: 2000, On the modulation of galactic cosmic ray intensity during solar activity cycles 19, 20, 21, 22 and early 23. *Geophys. Res. Lett.* **27**, 2453.

Verbanac, G., Vršnak, B., Živković, S., Hojsak, T., Veronig, A.M., Temmer, M.: 2011, Solar wind high-speed streams and related geomagnetic activity in the declining phase of solar cycle 23. *Astron. Astrophys.* **533**, A49. [DOI](#).

Webber, W.R., Lockwood, J.A.: 1988, Characteristics of the 22-year modulation of cosmic rays as seen by neutron monitors. *J. Geophys. Res.* **93**, 8735.

Wilson, R.M.: 1988, Bimodality and the Hale cycle. *Solar Phys.* **117**, 269. [DOI](#). [ADS](#).

Zharkova, V.V., Shepherd, S.J., Popova, E., Zharkov, S.I.: 2015, Heartbeat of the Sun from Principal Component Analysis and prediction of solar activity on a millenium timescale. *Sci. Rep.* **5**, 15689. [DOI](#). [ADS](#).

Publisher's Note Springer Nature remains neutral with regard to jurisdictional claims in published maps and institutional affiliations.